# Accuracy Enhancement in Optical Wireless Positioning Via Parametric Spectral Estimation

Zhibin Liu†, Jorik De Bruycker‡, Nobby Stevens ‡, Miguel Heredia Conde†
† Institute for High-Frequency and Communication Technology (IHCT), University of Wuppertal, Wuppertal, Germany
‡ Department of Electrical Engineering (ESAT), KU Leuven, Ghent, Belgium
zhliu@uni-wuppertal.de •jorik.debruycker@kuleuven.be• nobby.stevens@kuleuven.be • herediaconde@uni-wuppertal.de

***Abstract*—The advancement of high-speed and high-power Light-Emitting Diodes (LED) has paved the way for the widespread implementation of Visible Light Positioning (VLP) and Optical Wireless Positioning (OWP). Time Difference of Arrival (TDoA) techniques do not require synchronism between emitters and receivers. However, in TDoA, accurate time difference estimation becomes the key to accurate positioning. Prior work in OWP often neglects Non-Line-of-Sight (NLoS) contributions when modeling the scene response function. In contrast, we adopt an NLoS-aware model and solve the estimation problem in frequency domain via a fast and robust spectral estimation method. Leveraging both ideal model-based simulations and realistic raytracing software, we demonstrate that our approach allows for time difference estimation with machine precision, in the absence of secondary reflections. In the NLoS scenario, our method yields a reduction of the 95th percentile positioning error from $9.5\,\mathrm{cm}$ to $5.5\,\mathrm{cm}$ over Gaussian pulse fitting in a $1\,\mathrm{m} \times 1\,\mathrm{m}$ experimental frame. Furthermore, our method achieves a significantly higher estimation rate, making it highly suitable for real-time applications.**

***Index Terms*—Optical Wireless Positioning, Visible Light Positioning, Time Difference of Arrival, Parametric Spectral Estimation**

## I. Introduction

Indoor positioning technology has seen widespread adoption across various industries over the past few years and has become increasingly significant in our daily lives. Positioning technology that employs a light source in the Near-Infrared (NIR) wavelength region or visible light is known as Optical Wireless Positioning (OWP) [1], [2], while systems based specifically on visible light are termed Visible Light Positioning (VLP) [3]–[5].

Several techniques are employed in VLP systems. Primary trilateration methods are based on the Time of Arrival (ToA) [6], Time Difference of Arrival (TDoA) [7], and the Received Signal Strength (RSS) algorithms [8]. In addition, triangulation techniques, such as the Angle-of-Arrival (AOA)-based algorithm and image sensors (IS)-based methods [9], [10], are also common. While Line-of-Sight (LoS) is the primary signal propagation mode in VLP, Non-Line-of-Sight (NLoS) effects significantly impact accuracy, particularly in complex indoor environments [5]. The effect of multipath reflections on the performance of indoor VLP systems has been explored in [11]. Additionally, in [2], Keskin *et al.* successfully replaced Radio Frequency (RF)-based positioning systems with VLP, but also acknowledged that NLoS must be taken into account in the design of the VLP system. Zhou *et al.* reveal the performance limitations of VLP systems in NLoS propagation environments through Fisher information analysis in [12]. Furthermore, in [13], a comprehensive analysis of LED-based VLP systems is presented in terms of accuracy, complexity, cost, and commercial feasibility, highlighting that low-accuracy positioning at the edges or corners deserves to be investigated.

NLoS is typically regarded as a form of Multipath Interference (MPI), a major challenge in Time-of-Flight (ToF) systems. In this realm, parametric spectral estimation has shown success in retrieving multiple paths. In [14], a novel framework called Simultaneous Phase Unwrapping and Multipath Interference Cancellation (SPUMIC) was introduced, which addresses both phase unwrapping (PUW) and multipath interference cancellation (MIC) using spectral estimation techniques. In SPUMIC, MPI is modeled as a sum of a direct (LoS) and an indirect (NLoS) path. To tackle MPI, Fuchs proposed a model for estimating and compensating for MPI in [15], assuming that all reflective surfaces behave as Lambertian radiators. This model simulates interference to correct ToF camera measurements. Although this approach improves accuracy, its high computational demands make it unsuitable for real-time applications. Bhandari *et al.* developed a more computationally efficient, closed-form, non-iterative solution based on spectral estimation theory. Their approach requires $2K+1$ frequency measurements to recover depth and amplitude information for each of the $K$ paths. The method provides a practical, real-time solution for MPI correction without requiring iterative optimization, making it applicable for real-time scenarios [16], [17]. Heredia Conde *et al.* proposed a fast multipath estimation approach for the Continuous-Wave(CW) ToF camera based on the matrix pencil method [18]. Harmonic distortions in the acquired measurements can degrade estimation accuracy and lead to failure. Superior performance can be achieved by combining parametric spectral estimation with harmonic cancellation techniques in CW-ToF, effectively improving multipath separation and robustness [18].

The limited research on the effects of NLoS in VLP, combined with the notable success of parametric spectral

This work has been partially funded by the Deutsche Forschungsgemeinschaft (DFG, German Research Foundation) – project number 513531607 and by means of the Central Europe Leuven Strategic Alliance (CELSA) project CELSA-22-205: "Positioning by means of Optical Wireless timE diffeRences (POWER)."

estimation methods in retrieving multipath information in ToF applications, motivates this study. Our approach eliminates the need for detailed scene modeling, making it more adaptable and robust in diverse environments. Our contributions include:

1) Closed-form-solution instead of time-domain peak detection: Unlike classical Gaussian pulse fitting (GP) or other approaches in time domain, our work applies frequency-domain parametric spectral estimation to retrieve LoS and NLoS components, significantly enhancing TDoA localization accuracy.

2) Theoretical and practical integration: Our work combines theoretical rigor with experimental validation, using both mathematical modeling (Fig.1) and raytracing simulations (Fig.3). This dual approach not only enhances the robustness of our findings but also provides actionable insights for real-world implementation. The experimental results (Fig.4) are obtained in a $1\,\mathrm{m} \times 1\,\mathrm{m}$ experimental frame.

3) Filling a research gap: While parametric spectral estimation is widely used in ToF-based systems, its potential for mitigating MPI in TDoA-based localization, especially in OWP systems, remains largely unexplored.

## II. Mathematical Model

### A. A General Sensing Model

In a general system, the Scene Response Function (SRF) to modulated light *h(t)*, can be interpreted as a system's response to stimuli. This is often expressed using convolution:

$$r(t) = (s * h)(t) = \int_{-\infty}^{\infty} s(\tau) \cdot h(t-\tau)\, d\tau, \tag{1}$$

where *s(t)* and *r(t)* are the transmitted and received signals respectively. In many prior works, only the LoS contribution is considered in the VLP scenario, while the NLoS paths are often neglected. When *K* propagation paths are considered, the SRF can be modeled as a weighted sum of shifted Dirac delta functions [19]:

$$h(t) = \sum_{k=0}^{K-1} \Gamma_k \delta\left(t - t_k\right), \quad 0 \le t_k < T, \tag{2}$$

where $\Gamma_k$ and $t_k$ represent the amplitude and the time stamp of the $k^{th}$ path respectively. Here, *T* is the length of the observation period.

Convolution in the time domain is equivalent to element-wise product in the Fourier domain, meaning that equation (1) can be expressed as $\hat{r}(\omega) = \hat{h}(\omega) \cdot \hat{s}(\omega)$ in the Fourier domain. Due to physical limitations, almost all optical systems are approximately bandlimited [17], [19]. The bandlimited approximation with bandwidth $\Omega$ will be used. Fourier samples of a train of Dirac delta functions can be modeled as a sum of cisoids [19]. For any frequency $\omega \in \Omega$, $h(t)$ in (2) in the Fourier domain can be represented as:

$$\hat{h}(\omega) = \frac{\hat{r}(\omega)}{\hat{s}(\omega)} = \sum_{k=0}^{K-1} \Gamma_k e^{j\omega t_k} \tag{3}$$

We assume that *m* uniform frequency measurements $y(\omega_i) = \hat{r}(\omega_i) + \hat{n}_i$ are obtained, where $\hat{n}_i$ is the Gaussian noise in the $i^{th}$ measurement and $\hat{n}_i$= $\mathcal{F}(n_i)$, $\mathcal{F}$ denotes Fourier transform. Due to the maximal incoherence between the Fourier basis and Dirac delta functions, the direct acquisition of Fourier samples constitutes an optimal sampling procedure. The fundamental frequency is defined by $\omega_0 = \frac{2\pi}{T}$. The sensing model hence follows:

$$\tilde{\hat{h}}\left(\omega_i\right) = \frac{y(\omega_i)}{\hat{s}\left(\omega_i\right)}, \quad y(\omega_i) = \hat{s}\left(\omega_i\right) \sum_{k=0}^{K-1} \Gamma_k e^{j\omega_i t_k} + \hat{n}_i \quad \text{with :}$$
$$\omega_i = i\omega_0, \omega_i \in \Omega, i \in \left\{ -\left\lceil \frac{m-1}{2} \right\rceil, \ldots, 0, \ldots, \left\lfloor \frac{m-1}{2} \right\rfloor \right\} \tag{4}$$

To retrieve *K* paths, $\{\Gamma_k, t_k\}_{k=1}^{K}$, in (4), at least $m \ge 2K+1$ measurements are required. Prony's method can be employed to address this problem [20]. The matrix pencil method offers a fast and robust closed-form estimate of $\{\Gamma_k, t_k\}_{k=1}^{K}$ [22]. The oversampling factor is defined by $q = \frac{|m|-1}{2K}$, $q \in \mathbf{N}$.

### B. TDoA Via Parametric Spectral Estimation

Given the known positions of *n* receivers, the simplest NLoS scenario assumes two propagation paths *K*=2. The time of arrival for NLoS is modeled as:

$$t_{\mathrm{NLoS},n,\mathrm{ref}} = t_{\mathrm{LoS},n,\mathrm{ref}} + \Delta t_{\mathrm{d},n,\mathrm{ref}}, n \in [1,2,3,...] \tag{5}$$

where $t_{\mathrm{NLoS},n,\mathrm{ref}}$ and $t_{\mathrm{LoS},n,\mathrm{ref}}$ denote the ToA values of the NLoS and LoS components relative to a reference signal, which can be acquired in a calibration experiment. The term $\Delta t_{\mathrm{d},n,\mathrm{ref}}$ represents the time difference between these paths. The TDoA method relies on the time difference between the received and reference signals. Applying the Fourier transform to the received signal, $\hat{r}_{\mathrm{NLoS}}(\omega)$, and normalizing it by the Fourier transform of the convolution kernel (reference signal, $\hat{r}_{\mathrm{ref}}(\omega)$), results in the Fourier-domain deconvolved signal:

$$\tilde{\hat{h}}_{n,\mathrm{ref}}\left(\omega\right) = \frac{\hat{r}_{\mathrm{NLoS},n}(\omega)}{\hat{r}_{\mathrm{ref}}(\omega)} \tag{6}$$

The right-hand side can be expressed as a sum of sinusoidal components (complex exponentials), which can be efficiently solved using the Matrix Pencil Method [21], [22]. We define $\mathcal{M}$ as the matrix pencil algorithm. The estimated time and amplitude values are given by:

$$\left\{t_{n,\mathrm{ref},k}, \Gamma_{n,\mathrm{ref},k}\right\}_{k=1}^{K} = \mathcal{M}(\tilde{\hat{h}}_{n,\mathrm{ref}}\left(\omega\right); K, T, L, \Omega) \tag{7}$$

Where *K* is the number of paths, *T* is the signal period, *L* represents the pencil parameter, and $\Omega$ represents the bandwidth of bandlimited approximation. The path $P_1$ (most prominent) is considered as the LoS path and path $P_2$ as the sum of NLoS paths. The ToA estimates are:

$$t_{n,\mathrm{ref,LoS}} = t_{n,\mathrm{ref},1},\ t_{n,\mathrm{ref,NLoS}} = t_{n,\mathrm{ref},2} \tag{8}$$

The time difference for different receivers $\Delta t_{\mathrm{Rx},u,v}(u, v \in n$, where $u \ne v)$ is then:

$$\Delta t_{\mathrm{Rx},u,v} = t_{u,\mathrm{ref,LoS}} - t_{v,\mathrm{ref,LoS}} \tag{9}$$

By leveraging this model and the matrix pencil algorithm ($\mathcal{M}$), we can disentangle the LoS component in the presence of NLoS contributions. Equation (9) further allows LoS-TDoA computation for different received signals relative to the same reference signal. This procedure avoids errors due to NLoS contributions in the TDoA estimation, thereby improving localization accuracy and bringing it closer to the precision achieved under LoS conditions.

## III. Ideal Model-based Simulation and Realistic Raytracing Software Simulation

### A. Ideal Model-based Simulation

In practice, the received signal typically exhibits an overshoot because of the contribution of the higher-order filter response [23]. However, for simplicity in simulation, both the transmitted and received signals are modeled as Gaussian pulses, as usually done in Light Detection And Ranging (LiDAR) systems [24].

In the simulation, the transmitted Gaussian pulse, $s_G(t)$, and the received pulse train, $r_G(t)$, are modeled as follows:

$$s_G(t) = Ae^{-\frac{(t-t_0)^2}{2\sigma^2}}, r_G(t) = \sum_{k=0}^{K-1} \Gamma_k s_G(t-t_k), \qquad (10)$$

where $A$ is the amplitude of the pulse, $t_0$ is a reference time (center of the pulse), $\sigma$ is the pulse width, $K$ is the number of the received paths, $\Gamma_k$ and $t_k$ denote the amplitude and the time shift of the $k^{\text{th}}$ path respectively.

For the simulation, we consider a signal with a period $T$=20 ns and $K$=10 paths. The randomly generated parameters $\{\Gamma_k, t_k\}_{k=1}^{K}$ are then estimated by the matrix pencil method. The reconstructed signal and the retrieved parameters are shown in Fig.1 and Table I, respectively. In the absence of noise, the proposed approach enables time difference estimation with machine precision.

Additionally, we investigated the effect of noise level on the estimation error of time, $t_k$, amplitude, $\Gamma_k$, and reconstructed signal, $r_G$, under different oversampling factors $q$. The results are presented in Fig. 2. As the Signal-to-Noise Ratio (SNR) increases, the Mean Squared Error (MSE) decreases linearly, indicating that the Cramér-Rao Bound (CRB) is approached.

TABLE I
MSE of the vectors of reconstructed time locations and amplitudes, and of the reconstructed signals over 100 noise realizations in Fig.1 ($K$ = 10).

| SNR [dB] | MSE $\left\{\tilde{t}_k\right\}_{k=1}^{K}$ | MSE $\left\{\tilde{\Gamma}_k\right\}_{k=1}^{K}$ | MSE $\{\tilde{r}_G\}$ |
|---|---|---|---|
| 20 | 110.86 | $7.86\times10^{-1}$ | $4.71\times10^{-2}$ |
| 40 | $3.75\times10^{-4}$ | $2.8\times10^{-3}$ | $4.37\times10^{-4}$ |
| 60 | $3.07\times10^{-6}$ | $2.43\times10^{-5}$ | $4.34\times10^{-6}$ |
| $\infty$ | $4.19\times10^{-28}$ | $1.41\times10^{-27}$ | $9.72\times10^{-28}$ |

### B. Realistic Raytracing Software Simulation

In order to assess the impact of NLoS contributions in the VLP system, for example, due to walls, the SRF was first simulated in raytracing software (TracePro) in a real scenario with diffuse reflecting walls. The receivers are positioned at a height of 124 cm in a 1 m×1 m square in correspondence

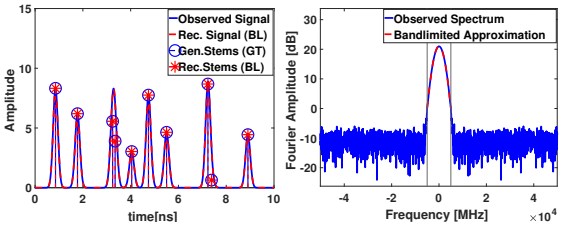


(a) Observed and reconstructed signal (b) Spectrum

Fig. 1. Observed and reconstructed signal and the Fourier spectrum. (a) 10 randomly-generated times and amplitudes (blue stems) are utilized to model the observed signal (blue line). The times and amplitudes obtained using our method and the reconstructed signals are represented as red stems and red dashed lines, respectively. (b) Fourier spectrum and the limited bandwidth $\Omega$ in red dashed line.

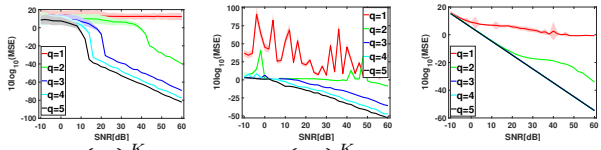


(a) MSE $\left\{\tilde{t}_k\right\}_{k=1}^{K}$ vs. SNR (b) MSE $\left\{\tilde{\Gamma}_k\right\}_{k=1}^{K}$ vs. SNR (c) MSE $\{\tilde{r}_G\}_{k=1}^{K}$ vs. SNR

Fig. 2. MSE of reconstructed time (a), amplitude (b), and signal (c) versus SNR for different oversampling factors $q \in [1, 5]$. The original set of parameters $\{\Gamma_k, t_k\}_{k=1}^{K}$ was the same used in Fig. 1, with $K$=10. The solid lines are mean computed over 100 noise realizations, while the shaded areas indicate the range between the mean minus and plus two times standard deviations.

with the measurement setup described in [23]. The simulation assumes a 1.2 m×1.2 m room with white reflective walls, thus 10 cm wider than the positions of the receivers at each side of the square. The walls are modeled as a Lambertian diffuse reflecting surface with 80% reflectance, a representative value for typical white paint [25], [26]. The radiation pattern of the transmitter is applied in the simulation as provided by the manufacturer and is used to simulate the propagation of $10^6$ rays, employing importance sampling to the target receiver from both the laser source and reflections at the walls. The transmitter is positioned in the center of the room and the SRF is simulated for one of the receivers at the corners of the room. Instead of generating ten random paths, as in Section III-A, with the help of the raytracing software, we successfully simulated the SRF of the real scenario and selected the first ten paths for testing, where $K$=1 is the LoS.

The results of retrieving two paths and ten paths using our method are shown in Fig. 3. For the case with two paths, the second path is considered to be the sum of the NLoS components and is represented as a red star stem in Fig. 3(a). In Fig. 3(b), all ten stems are accurately depicted. In the absence of noise, our proposed method effectively eliminates the effects of NLoS in the TDoA system, and allows also for accurate reconstruction of the received signals in the LoS-only scenario. Additionally, we observe that, as the number of paths $K$ retrieved using our method approaches the true number of paths, the accuracy of the results improves.

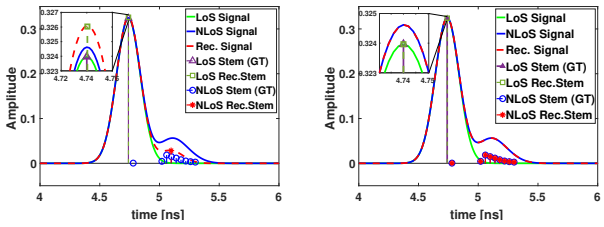


(a) Reconstruction for $K$=2 vs. GT (b) Reconstruction for $K$=10 vs. GT

Fig. 3. Simulated SRF with ten paths (blue stems), when the transmitter is positioned in the center of the rooms. Using our method to retrieve two paths (a) and all ten paths (b) reconstructs the signal with the depicted time and amplitude. The reconstructed signal is represented as a red dashed line. When tracking only two paths (a), a dark green box represents the estimated LoS contribution, while a red star denotes the sum of the NLoS contributions. When tracking ten paths (b), the dark green box again represents the LoS contribution, but nine red stars are used to depict the individual NLoS components.

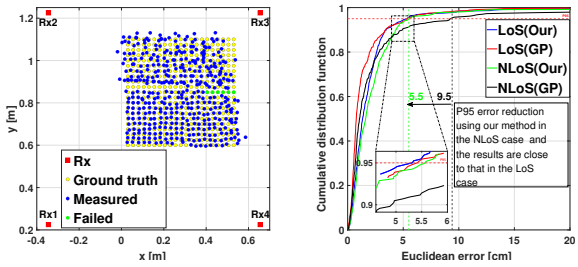


(a) TDoA positioning results using our method in the NLoS case (b) The P95 positioning error

Fig. 4. TDoA Positioning results and the P95 Positioning error. (a) Comparison of the TDoA results using our method with the test points in the case of NLoS. The green points indicate the failure of parametric spectral estimation due to the distortion of the signal at these test points. (b) Cumulative distribution function of the positioning error comparing our method and the GP method for the LoS case and the NLoS case.

## IV. Experimental Setup and Results

The experimental setup is at a range of $1.24\,\mathrm{m}$ with four photodetectors mounted on a frame of size $1\,\mathrm{m}\times1\,\mathrm{m}$. The experimental setup and its specifications are described in detail in [23]. The 441 test points are distributed uniformly over a $50\,\mathrm{cm}\times50\,\mathrm{cm}$ square grid. In [23], the received signals are modeled as Gaussian pulses, and the time $t_0$ is retrieved by GP. In order to simplify the calibration process, the measurements when the transmitter is at the center are used to compensate for all measurement points. The same dataset is used in our proposed method. Unlike the ideal simulation scenario, the practical implementation of our method for retrieving NLoS paths requires careful consideration due to the unknown number of paths $K$ and the device specifications. The photodiode used as a receiver has an analog bandwidth of only $150\,\mathrm{MHz}$, which imposes a significant limitation. In our experiments, the signals are collected within a period $T$=$20\,\mathrm{ns}$, corresponding to a fundamental frequency $f_0$=$\frac{1}{T}$=$50\,\mathrm{MHz}$. The maximum frequency used for bandlimited approximation cannot exceed the photodiode's maximum analog bandwidth of $150\,\mathrm{MHz}$, which limits the number of uniform frequency measurements to $m$=7. Consequently, at most $K$=3 can be retrieved in the experimental framework. In many test points, $K$=3 yielded unrealistic negative amplitudes ($\Gamma$). Therefore we only consider the case $K$=2 for the whole experiment.

When Rx1 is taken as the reference signal, the calibration results calculated by the GP method [23] and our proposed method (8) are nearly identical. This demonstrates that the sum of the contribution from NLoS paths can be estimated via the parametric spectral estimation method, even when the number of paths $K$ is unknown, following a similar approach to analyzing the MPI of ToF cameras to that in [14]. The calibration measurement results obtained from both methods are presented in Table II.

To estimate the effect of NLoS contributions, two whiteboards with a width of $55\,\mathrm{cm}$ are placed in the corner close to Rx4. The experimental setup is illustrated in Fig. (14) of [23]. Data from the same 441 test points are collected

TABLE II
Comparison of Calibration Measurement Results at the Center of the Grid.

| TDoA | Ours [ps] | GP [ps] |
|---|---|---|
| Rx2-Rx1 | 147.7 | 148.1 |
| Rx3-Rx1 | 151.8 | 155.4 |
| Rx4-Rx1 | 186.0 | 188.4 |

TABLE III
Average Runtime Comparison over 100 Runs for 441 Samples in LoS and NLoS Scenarios.

| Method | LoS | NLoS |
|---|---|---|
| Ours [ms]) | 4.6 | 5.4 |
| GP [ms] | 26.6 | 34.1 |
| Speed-up | **5.7x** | **6.3x** |

under the NLoS experimental setup. By inputting the collected reference data and received data from the NLoS scenario into (6)-(9), we successfully eliminate the NLoS contribution to localization, approximating the NLoS localization accuracy to that of the LoS case. However, at specific receiver locations, the received signal exhibits distortion due to overshoot and time-domain cropping, resulting in the failure of parametric spectral estimation, as indicated by the green points in Fig.4(a). In Section III-A we note that the overshoot arises from the contribution of higher-order filter responses in practical systems, deviating from the ideal Gaussian pulse model used in simulations, particularly in the NLoS scenarios where MPI further complicates the waveform. When the acquisition time is too short to fully capture the overshoot and the NLoS components, the collected signal becomes incomplete, truncating critical NLoS components or their tails. This time-domain truncation disrupts the Fourier-domain analysis based on the matrix pencil method. Importantly, this distortion is not a fundamental limitation of our method, which performs robustly under ideal conditions (in Section III-A), but rather a consequence of constraints in the data acquisition campaign, specifically resulting from the combination of overshoot and insufficient acquisition time. By extending the signal duration and using higher-performance experimental devices, the impact of distortion can be mitigated, improving the accuracy and robustness of the estimation.

The cumulative distribution function of the localization error, shown in Fig. 4, illustrates the positioning performance of TDoA in the LoS and NLoS scenarios attained employing the GP method and our method, respectively. Our method

achieves a P95 value of $5.3\,\mathrm{cm}$, closely matching the P95 value of $5.4\,\mathrm{cm}$ obtained using the GP method. However, in the case of NLoS, our method is able to eliminate the aggregated effect of NLoS, improving the P95 result from $9.5\,\mathrm{cm}$ to $5.5\,\mathrm{cm}$, which verifies the superiority of our algorithm in real scenarios. In addition to accuracy improvements, we also compared the computational efficiency of the GP method and our proposed method. The average runtime over 441 test positions and 100 runs per position in both LoS and NLoS scenarios is shown in Table III. The estimation rate, defined as the number of position estimates computed per second, is a key metric for evaluating real-time performance. Our method achieves an estimation rate of approximately $217\,\mathrm{Hz}$ in the LoS scenarios and $185\,\mathrm{Hz}$ in the NLoS scenarios, significantly outperforming the GP method, with a 5.7 times speed-up and 6.3 times, respectively.

## V. Conclusion

In this paper, we investigate the impact of NLoS contributions on a TDoA-OWP system. Contrary to the classical waveform fitting methods that analyze signals in the time domain, our approach utilizes a non-iterative parametric spectral estimation method in Fourier domain to account for NLoS contributions, thereby enhancing localization accuracy by mitigating NLoS effects in the TDoA measurements. Ideal simulations and realistic raytracing software demonstrate that our proposed method achieves machine precision without the influence of secondary reflections. In practical NLoS experimental scenarios, our method reduces the P95 positioning error from $9.5\,\mathrm{cm}$ to $5.5\,\mathrm{cm}$, representing a $42\%$ improvement over the GP method. Furthermore, our method exhibited a significantly higher estimation rate, outperforming the GP method by 5.7 times in the LoS scenarios and 6.3 times in the NLoS scenarios. This combination of improved accuracy and computational efficiency makes our approach highly suitable for real-time position estimation in indoor environments. Moreover, the enhanced estimation rate is key for autonomous navigation, enabling rapid and reliable position updates essential for AGVs, mobile robots, and other real-time localization applications.

## References


[1] Ł. Januszkiewicz, J. Kawecki, R. Kawecki and P. Oleksy, "Wireless indoor positioning system with inertial sensors and infrared beacons," in 2016 10th European Conference on Antennas and Propagation (EuCAP), 2016, pp. 1-3.

[2] M. F. Keskin, A. D. Sezer and S. Gezici, "Localization via Visible Light Systems," in Proceedings of the IEEE, vol. 106, no. 6, 2018, pp. 1063-1088.

[3] Z. Cui, Y. Wang and X. Fu, "Research on Indoor Positioning System Based on VLC," in 2020 Prognostics and Health Management Conference (PHM-Besançon), 2020, pp. 360-365.

[4] S. De Lausnay, L. De Strycker, J. -P. Goemaere, B. Nauwelaers and N. Stevens, "A survey on multiple access Visible Light Positioning," 2016 IEEE International Conference on Emerging Technologies and Innovative Business Practices for the Transformation of Societies (EmergiTech), Balaclava, Mauritius, 2016.

[5] Z. Liu, N. Stevens and M. Heredia Conde, "Visible Light Positioning Using Arrays of Time-of-Flight Pixels," in 2022 IEEE Sensors, Dallas, TX, USA, 2022, pp. 1-4.

[6] B. Kazimieras, and K. Borre, "Ubiquitous WiFi/GNSS positioning system-TOA based distance estimation," in Proceedings of the 21st International Technical Meeting of the Satellite Division of The Institute of Navigation (ION GNSS 2008), 2008, pp. 1773-1779.

[7] R. W. Boyd, "Location system for wireless local area network (WLAN) using RSSI and time difference of arrival (TDoA) processing," U.S. Patent No. 7,899,006. 1 Mar. 2011.

[8] Z. Hengzhou, L. Fuqiang and Z. Hao, "Indoor Location Service Based on Fingerprinting and Distance Relative Attenuation Model," 2014 Sixth International Conference on Measuring Technology and Mechatronics Automation, Zhangjiajie, China, 2014, pp. 341-344.

[9] M. S. Rahman, M. M. Haque and Ki-Doo Kim, "High precision indoor positioning using lighting LED and image sensor," 14th International Conference on Computer and Information Technology (ICCIT 2011), Dhaka, Bangladesh, 2011, pp. 309-314.

[10] K. Aalimahmoodi, A. Gholami and Z. Ghassemlooy, "An Image Sensor Based Indoor VLP System," 2018 9th International Symposium on Telecommunications (IST), Tehran, Iran, 2018, pp. 371-374.

[11] W. Gu, M. Aminikashani, P. Deng and M. Kavehrad, "Impact of multipath reflections on the performance of indoor visible light positioning systems," in J. Lightw. Technol., vol. 34, no. 10, pp. 2578-2587, May 2016.

[12] B. Zhou, Y. Zhuang and Y. Cao, "On the Performance Gain of Harnessing Non-Line-of-Sight Propagation for Visible Light-Based Positioning," in IEEE Transactions on Wireless Communications, vol. 19, no. 7, pp. 4863-4878, July 2020.

[13] Y. Zhuang et al., "A Survey of Positioning Systems Using Visible LED Lights," in IEEE Communications Surveys and Tutorials, vol. 20, no. 3, pp. 1963-1988, third quarter 2018.

[14] A. Kirmani, A. Benedetti and P. A. Chou, "SPUMIC: Simultaneous phase unwrapping and multipath interference cancellation in time-of-flight cameras using spectral methods," 2013 IEEE International Conference on Multimedia and Expo (ICME), San Jose, CA, USA, 2013, pp. 1-6.

[15] S. Fuchs, "Multipath Interference Compensation in Time-of-Flight Camera Images," 2010 20th International Conference on Pattern Recognition, Istanbul, Turkey, 2010.

[16] A. Bhandari, F. Micha, I. Shahram, R. Christoph, S. Mirko, and R. Ramesh, "Resolving multipath interference in kinect: An inverse problem approach." In SENSORS, 2014 IEEE, pp. 614-617. IEEE, 2014.

[17] A. Bhandari, A. M. Wallace, and R. Raskar, "Super-resolved time-of-flight sensing via FRI sampling theory," 2016 IEEE International Conference on Acoustics, Speech and Signal Processing (ICASSP), Shanghai, China, 2016.

[18] M. Heredia Conde, T. Kerstein, B. Buxbaum, and O. Loffeld, "Fast multipath estimation for PMD sensors," in 5th International Workshop on Compressed Sensing Theory and its Applications to Radar, Sonar, and Remote Sensing (CoSeRa 2018), 2018.

[19] S. C. Sánchez El Ryfaie and M. Heredia Conde, "Breaking the Limits of Gamma-Ray Spectrometry by Exploiting Sparsity of Photon Arrivals," 2020 28th European Signal Processing Conference (EUSIPCO), Amsterdam, Netherlands, 2021, pp. 2075-2079.

[20] P. Stoica and R.L. Moses, "Introduction to Spectral Analysis," Prentice Hall, 1997.

[21] A. Bhandari, M. Heredia Conde and O. Loffeld, "One-Bit Time-Resolved Imaging," in IEEE Transactions on Pattern Analysis and Machine Intelligence, vol. 42, no. 7, pp. 1630-1641, 1 July 2020.

[22] Y. Hua and T. K. Sarkar, "Matrix pencil method for estimating parameters of exponentially damped/undamped sinusoids in noise," in IEEE Transactions on Acoustics, Speech, and Signal Processing, vol. 38, no. 5, pp. 814-824, May 1990.

[23] J. D. Bruycker, J. Audenaert, S. R. Teli, S. Zvanovec, M. Heredia Conde, L. D. Strycker, N. Stevens. "An Experimental Testbed for the Performance Evaluation of Optical Time Difference of Arrival based Indoor Positioning." Journal of Lightwave Technology. 2024, pp. 1-10.

[24] X. Li, H. Wang, B. Yang, J. Huyan, L. Xu, "Influence of Time-Pickoff Circuit Parameters on LiDAR Range Precision." Sensors 2017, 17, 2369.

[25] J. A. Sanderson, "The Diffuse Spectral Reflectance of Paints in the Near Infra-Red," J. Opt. Soc. Am., vol. 37, no. 10, pp. 771–777, Oct 1947.

[26] M. Rea and I. E. S. of North America, "The IESNA Lighting Handbook: Reference and Application," ser. IESNA LIGHTING HANDBOOK. Illuminating Engineering Society of North America, 2000.